J. Fluid Mech. (1996), *vol.* 308, *pp.* 195–217

Effects of compressibility, pitch rate, and Reynolds number on unsteady incipient leading-edge boundary layer separation over a pitching airfoil

By P. GHOSH CHOUDHURI AND D. D. KNIGHT

Department of Mechanical and Aerospace Engineering, PO Box 909, Rutgers University, Piscataway, NJ 08855, USA

(Received 10 January 1995 and in revised form 18 July 1995)

The effects of compressibility, pitch rate and Reynolds number on the initial stages of two-dimensional unsteady separation of laminar subsonic flow over a pitching NACA-0012 airfoil have been studied numerically. The approach involves the simulation of the flow by solving the two-dimensional unsteady compressible laminar Navier–Stokes equations employing the implicit approximate-factorization algorithm of Beam & Warming and a boundary-fitted C-grid. The algorithm has been extensively validated through comparison with analytical and previous numerical results. The computations display several important trends for the 'birth' of the primary recirculating region which is a principal precursor to leading-edge separation. Increasing the non-dimensional pitch rate from 0.05 to 0.2 at a fixed Reynolds number and Mach number delays the formation of the primary recirculating region. The primary recirculating region also forms closer to the leading edge. Increasing the Mach number from 0.2 to 0.5 at a fixed Reynolds number and pitch rate causes a delay in the formation of the primary recirculating region and also leads to its formation farther from the airfoil top surface. The length scale associated with the recirculating regions increases as well. Increasing the Reynolds number from 10^4 to 10^5 at a fixed Mach number and pitch rate hastens the appearance of the primary recirculating region. A shock appears on the top surface at a Reynolds number of 10^5 along with the simultaneous formation of multiple recirculating regions near the leading edge.

1. Introduction

1.1. *Overview*

The aerodynamic characteristics (e.g. lift, drag and moment) of an airfoil in unsteady motion are significantly affected by the viscous boundary layer. Under certain conditions, the boundary layer on an airfoil in pitching motion separates from the airfoil surface, forming a large concentrated region of vorticity known as the dynamic stall vortex. This phenomenon is characterized by dramatic changes in the aerodynamic performance (e.g. a rapid change in the moment) of the airfoil, and is of significant interest for rotorcraft, for example.

The focus of the present research is the understanding of the initial ('incipient') stages of boundary layer separation from a pitching airfoil, with particular emphasis

on the details of the separation phenomenon near the leading edge. Improved understanding of the incipient stages of boundary layer separation may lead to methods for modification or control of the separation process.

1.2. *Literature review*

The phenomenon of unsteady flow separation on pitching airfoils is not yet completely understood. A number of recent research activities have focused on the study of the processes leading to the dynamic stall and the dynamic stall phenomenon itself. Comprehensive reviews of advances in the field of computational and experimental studies of dynamic stall have been presented by Carr (1988) and Carr & McCroskey (1992). Experimental studies have provided very important insights into the physics of the dynamic stall process. McCroskey, Carr & McAlister (1976) studied incompressible boundary layer separation using oil smoke visualization and described the three different types of boundary layer separation observed in the case of an oscillating airfoil. Acharya & Metwally (1990) categorized and quantified the sources of vorticity. Chandrasekhara & Ahmed (1991) obtained the instantaneous velocity measurements over an oscillating airfoil in a compressible medium which showed the formation of the separation bubble over the airfoil that persists until angles close to when the dynamic stall vortex forms and convects. Karim (1992) experimentally studied the evolution of the dynamic stall vortex in the vicinity of leading edge of a two-dimensional pitching airfoil using smoke wires and studied the pitch rate effects on the growth of the dynamic stall vortex. He also investigated the control of dynamic stall using suction. Chandrasekhara, Carr & Wilder (1994) used real-time point diffraction interferometry to study the compressible dynamic stall over an airfoil pitching at a constant rate and observed the appearance of small multiple shocks near the leading edge above the shear layer for free-stream Mach numbers above 0.4. Crisler, Krothapalli & Lourenco (1994) investigated the unsteady flow over an airfoil pitching at a constant rate using a Particle Image Velocimetry (PIV) system and identified the role of absolute instability of a separating shear layer in the dynamic stall process.

Computational studies have long been used to improve the understanding of the unsteady flow behaviour. Mehta (1977) computed the laminar flow past a oscillating airfoil at Reynolds numbers of 5×10^3 and 10^4 to gain insight into the mechanism of dynamic stall. Shih *et al.* (1992) observed that the leading-edge boundary layer separation leads to the formation of a vortical structure which dominates the aerodynamic performance. Ghia *et al.* (1992) and Yang *et al.* (1993) analysed the effect of modulated suction or injection in delaying the onset of dynamic stall over pitching NACA airfoils. Visbal (1991) presented investigations of flow control by boundary layer suction and a moving wall. He also investigated the effect of compressibility on dynamic stall and determined that an increase in Mach number reduces the stall delay (Visbal 1990). Currier & Fung (1992) found that with increasing unsteadiness the delay between static stall angle and dynamics stall onset decreases. Van Dommelen & Shen (1980) studied the unsteady separation process and identified the evolution of unsteady boundary layer structures by using a Langrangian approach. They found the unsteady laminar boundary layer equation to turn singular spontaneously at a stationary point.

Analytical studies have been very helpful in the fundamental understanding of unsteady separation and linking the physics with the experimental and numerical observations. Doligalski, Smith & Walker (1994) have reviewed some of the important studies conducted on vortex interactions and separation including dynamic stall.

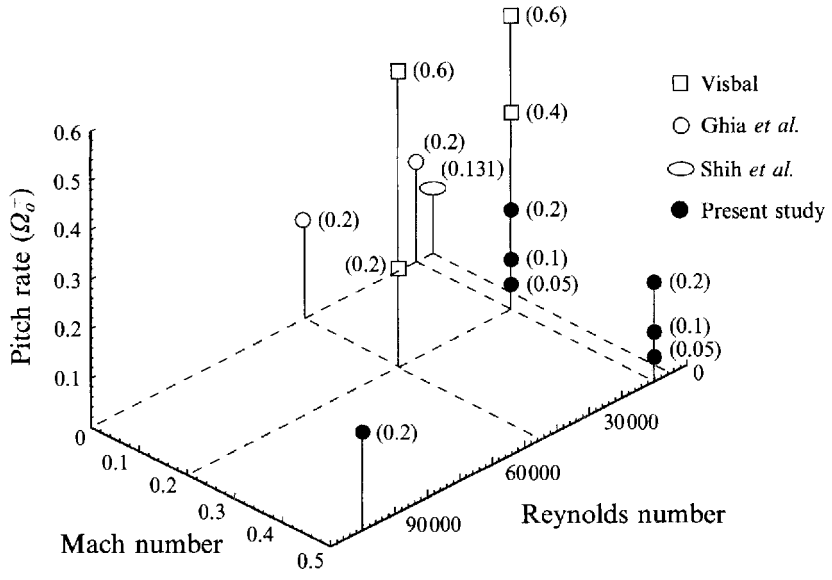

FIGURE 1. Points investigated in the three-dimensional parameter space (pitch rate value is shown in brackets).

Smith (1982, 1988) and Smith & Elliott (1985) described the linear and nonlinear instability of a leading-edge separation bubble and finite-time breakup of the boundary layer. Peridier, Smith & Walker (1991*a*,*b*) examined the interaction of a vortex with a boundary layer. Improved understanding of the temporal and spatial scales associated with the dynamic stall process have been obtained from these studies.

1.3. *Research objective*

The main objective of the present paper is improved understanding of the effects of compressibility, pitch rate and Reynolds number on the initial stages of unsteady leading-edge boundary layer separation for a pitching airfoil. An NACA-0012 airfoil has been selected, consistent with previous computational and experimental studies. The three-dimensional parameter space of Mach number, pitch rate and Reynolds number has been investigated. The seven points studied in the three-dimensional space are indicated by solid circles in figure 1. Some of the previous laminar Navier–Stokes simulations of a pitching airfoil of other researchers have also been indicated on the figure. Computations have been performed using the approximate-factorization algorithm of Beam & Warming (1978) employing a boundary-fitted grid system. The algorithm is implicit and second-order accurate in space and time. The airfoil is pitched about the quarter-chord axis. The flow conditions for the seven computed cases were chosen on the basis of simplicity and feasibility. The Reynolds numbers were selected to ensure laminar flow. The Mach numbers were chosen to obtain subsonic flow in one case and regions of supersonic flow in the other case. The studies were conducted with special emphasis on understanding the leading-edge separation, of course. The boundary layer separates near the trailing edge very early in the pitch-up motion, but for most of the cases it is the separation of the boundary layer near the leading edge which is responsible for the eventual dynamic stall process.

The previous study of Ghosh Choudhuri, Knight & Visbal (1994) at $Re_c = 10^4$, $M_\infty = 0.2$, and non-dimensional pitch rate $\Omega_o^+ = 0.2$ (where $\Omega^+ = \Omega c/U_\infty$, where Ω is the pitch rate in rad s^{-1}, c is the chord length, and U_∞ is the free-stream velocity)

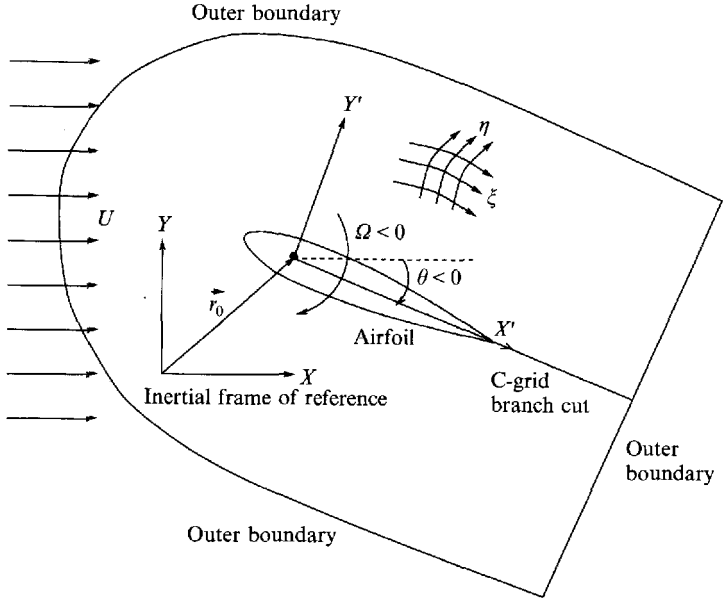

FIGURE 2. C-grid configuration and the computational boundaries.

reported the appearance of the primary recirculating region (a flow structure possessing vorticity with closed streamlines) to be a very important development leading to the separation process. The primary recirculating region eventually separates from the airfoil surface to give rise to the dynamic stall vortex. Therefore, the appearance of the primary recirculating region has been closely monitored in the present study.

This study differs from previous computational studies in the following aspects: it is a comprehensive study of the expanded three-dimensional parametric space of Mach number, pitch rate and Reynolds number; the initial stages of the development of the boundary layer leading to the development of the dynamic stall vortex have been studied.

2. Definition of the problem and details of computations

The focus of the research is understanding the effect of compressibility, pitch rate and Reynolds number on the incipient separation for viscous flow past a NACA-0012 airfoil pitching about the quarter-chord axis. The flow and C-grid configurations are shown in figure 2. The pitching motion of the airfoil which was initiated after the flow field had been fully established at $\alpha = 0°$ was defined by

$$\Omega(t) = \Omega_0(1 - \exp(-4.6t/t_0)) \tag{2.1}$$

where Ω is the pitch rate in rad s^{-1}, t_0 is the time at which Ω has reached 99% of the asymptotic value Ω_0. The functional form of $\Omega(t)$ provides a smooth acceleration of the airfoil to its asymptotic pitching rate during an effective time interval t_0. In this study, t_0 was set equal to $0.5c/U_\infty$, which corresponds to 4.57° of pitch. As indicated in §3, this ensures that the airfoil pitching rate has reached a constant value long before the incipient separation at the leading edge.

An extensive grid refinement study was conducted for each of the cases studied (details in §2.4). Complete details of the grids employed for the different cases are given in table 1. A total of seven cases were studied (figure 1). The accuracy of the

Case number	Reynolds number	Mach number	Pitch rate	Grid	N_ξ	N_η	$\Delta n/c$ ($\times 10^4$)	$\Delta s/c$ ($\times 10^3$)	N_{BL}
1	10^4	0.2	0.2	a	637	181	1.0	1.69	64
				b	1011	181	1.0	0.84	64
				c	637	325	0.5	1.69	112
2	10^4	0.2	0.1	a	1037	181	1.0	1.025	58
				b	2073	361	0.5	0.511	115
3	10^4	0.2	0.05	a	1037	181	1.0	1.025	58
				b	2073	361	0.5	0.511	115
4	10^4	0.5	0.2	a	1037	181	1.0	1.025	58
				b	2073	361	0.5	0.511	115
5	10^4	0.5	0.1	a	1037	181	1.0	1.025	58
				b	2073	361	0.5	0.511	115
6	10^4	0.5	0.05	a	2073	159	2.0	0.509	44
				b	4145	317	1.0	0.252	88
7	10^5	0.5	0.2	a	2073	337	0.05	0.509	124
				b	4145	673	0.025	0.252	247

TABLE 1. Details of the grids: N_ξ, Number of points in ξ-direction; N_η, Number of points in η-direction; Δn, average normal distance of points next to airfoil; Δs, minimum tangential distance of points on airfoil; N_{BL}, number of points in boundary layer measured normal to airfoil surface at mid-chord for $\alpha = 0°$.

computations was assessed for each case based on the comparison of the results for two grids with successive refinement. A non-dimensional time step $\Delta t^+ = \Delta t U_\infty / c = 1.0 \times 10^{-3}$ was employed for all cases. The computed results were found to be insensitive to the time step selected.

The seven cases were chosen to study and understand the effects of compressibility, pitch rate and Reynolds number on the incipient separation process. In cases 1–3 and 4–6, the pitch rate is decreased while keeping the Reynolds and Mach numbers constant, while in cases 1 and 4, 2 and 5, 3 and 6, the Mach number is increased from 0.2 to 0.5 while the Reynolds number and pitch rate are fixed. Cases 4 and 7 are computed at different Reynolds number while the Mach number and the pitch rate are fixed. The Reynolds numbers chosen for this study are in the laminar flow region (Carr & Chandrasekhara 1995).

2.1. *Governing equations*

The governing equations are the two-dimensional unsteady compressible laminar Navier–Stokes equations written in strong conservation form (Steger 1978). The flow equations are written in an inertial frame of reference and the motion of the airfoil is included through a general time-dependent coordinate transformation $\xi = \xi(x, y, t)$, $\eta = \eta(x, y, t)$, and $\tau = t$ (figure 2). The flow variables are non-dimensionalized using the dimensional reference quantities c (chord length), ρ_∞ (density), and u_∞ (free-stream velocity). The dynamic molecular viscosity is assumed to satisfy Sutherland's relation (White 1974). The temperature, pressure and density satisfy the ideal gas equation. The Prandtl number is constant ($Pr = 0.73$).

2.2. *Numerical algorithm*

The implicit approximate-factorization method of Beam & Warming (1978) is employed to solve the governing equations on a structured, boundary-fitted grid. The algorithm is implemented in the delta form with central spatial and trapezoidal

temporal differencing to achieve second-order spatial and temporal accuracy. Fourth-order explicit and second-order implicit numerical dissipation terms (Pulliam 1986) are incorporated to eliminate spurious numerical oscillations. The sensitivity of the results to the values of the dissipation coefficients was assessed (Ghosh Choudhuri *et al.* 1994) to check that the dissipation terms do not affect the solution. The Geometric Conservation Law (GCL) (Thomas & Lombard 1979) is implemented in the algorithm to eliminate the grid-movement-related errors in the governing equations due to the pitch-up motion of the airfoil.

2.3. *Boundary conditions*

Along the boundaries of the computational domain, suitable boundary conditions are incorporated. The C-grid has numerical boundaries at the airfoil surface, the outer boundary, and on a branch cut in the wake region (figure 2). At the airfoil surface, the no-slip condition is applied to the velocity and the temperature is determined from the adiabatic condition (the normal temperature gradient is zero at the surface). The normal pressure gradient is obtained from the momentum equation and incorporates the effect of the airfoil motion (Visbal & Shang 1989; Visbal 1990). At the C-grid branch-cut, the flow variables are solved implicitly and the periodicity condition is imposed. At the outer boundary of the computational domain, a one-dimensional unsteady Method of Characteristics boundary condition is employed (Thomas & Salas 1986). The boundary conditions are imposed explicitly except at the C-grid branch-cut. The outer boundary is defined at a sufficiently large distance from the airfoil to ensure accuracy of this boundary condition (Ghosh Choudhuri *et al.* 1994).

The code was developed from the original code of Visbal (1986*a*,*b*). Modifications include the incorporation of a C-grid, the Method of Characteristics boundary condition at the outer boundary, and the Geometry Conservation Law.

2.4. *Grid generation*

The boundary-fitted C-grid was generated by the hyperbolic grid generation code developed by Kinsey & Barth (1984). The hyperbolic grid generation solver produces nearly orthogonal computational grids over arbitrary two-dimensional bodies and provides good control of the grid spacing. Detail of the algorithm can be found in Steger & Chaussee (1980). The distribution of points on the airfoil and the wake region, normal grid spacing at the airfoil surface, the outer boundary distance, the number of points in the ξ- and η-directions, and the exponential stretching factor in the η-direction are specified to obtain the computational grid. The grid is fixed with respect to the airfoil and therefore pitches with it.

2.5. *Validation of the algorithm*

A series of steady and unsteady test computations established the accuracy of the algorithm, including the effects of spatial and temporal resolution, damping coefficients, and the outer boundary distance of the computational domain from the airfoil surface. The test computations included a flat-plate laminar boundary layer, a stationary NACA-0012 airfoil, and a pitching NACA-0015 airfoil. Details are presented in Ghosh Choudhuri *et al.* (1994). A separate computation was also conducted using an unstructured grid algorithm for Case 1 (Ghosh Choudhuri *et al.* 1994). The streamline plots showed close agreement between the structured and unstructured grid computations, which lends substantial credibility to the accuracy of the algorithm.

Extensive grid refinement studies were performed for each computation that indicated achievement of highly accurate solutions. Computations were performed on

Case number	Root-mean-square error (%)	Range of α (deg.)
1	1.4	$0 < \alpha < 22.5$
2	1.1	$0 < \alpha < 21$
3	1.6	$0 < \alpha < 16.5$
4	1.6	$0 < \alpha < 25.5$
5	2.1	$0 < \alpha < 21$
6	1.3	$0 < \alpha < 18$
7	3.8	$0 < \alpha < 19.5$

TABLE 2. Comparison of lift, drag and moment coefficients between the different grids.

two separate grids for each case, with Grid b representing a two-fold refinement of the grid in *both* the ξ- and η-directions relative to Grid a (except in Case 1, where Grids b and c represent an approximately by twofold refinement of the grid in either the ξ- or η-direction relative to Grid a). A comparison of lift (c_l), drag (c_d), and moment ($c_{m_{ac}}$) coefficients showed very close agreement between successively refined grids for all the seven cases as shown in table 2. The flow variables for the two grids were also compared at different locations in the flow field. The agreement between the grids was found to be excellent for all cases. Typically, the flow variables agreed to within 3–4% for the two grids.

3. Results

The flow structures observed in the seven cases studied are described in the following subsections. The results presented here correspond to Grid b. The instantaneous streamlines are plotted based on a reference frame attached to the airfoil. (The instantaneous streamlines have not been plotted to scale in order to show all flow details.) The origin of the coordinate axis is the quarter-chord point. The airfoil-attached reference frame allows an unambiguous definition of forward and reversed flow within a thin unseparated boundary layer, since the velocity of the fluid at the airfoil surface is zero. Forward flow is defined as fluid moving toward the trailing edge, and reversed flow indicates fluid moving toward the leading edge.

3.1. *Case 1* : $Re_c = 10^4$, $M_\infty = 0.2$, $\Omega_o^+ = 0.2$

The details of the flow field for this case have been presented in Ghosh Choudhuri *et al.* (1994). The instantaneous streamlines at $\alpha = 14.5°$, 19.5°, and 22.5° are shown in figure 3(*a–c*). At $\alpha = 14.5°$, the flow on the upper surface in the vicinity of the leading edge has a thin reversed flow region extending to the 7% chord position. A clockwise-rotating primary recirculating region can be seen near the leading edge on the upper surface at $\alpha = 19.5°$. The counterclockwise-rotating secondary recirculating region appears beneath the primary recirculating region and a clockwise-rotating tertiary recirculating region between the leading edge and the primary recirculating region at $\alpha = 22.5°$. The emergence of the primary recirculating region is traced to the appearance of a pair of critical points (which are defined as points in the velocity field where $u = v = 0$ in a reference frame attached to the airfoil) within the flow field at $\alpha = 14.99°$ ($t = 1.416$) at the 18% chord location and a distance $2.5 \times 10^{-3}c$ above the airfoil surface. In figure 4, the close-up of the instantaneous streamlines at $\alpha = 15°$ shows the structure of the primary recirculating region just after its birth. The primary and secondary recirculating regions interact with each other to eject the fluid close

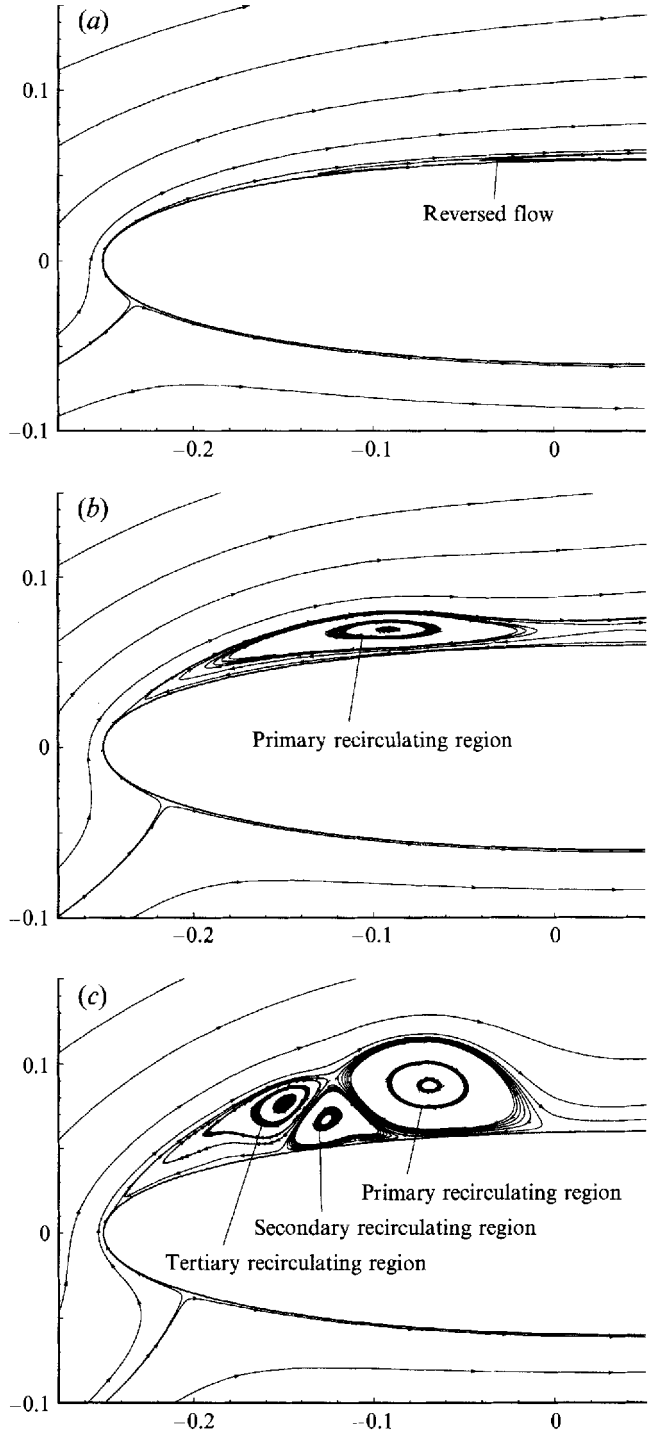

FIGURE 3. Instantaneous streamlines ($Re_c = 10^4$, $M_\infty = 0.2$, $\Omega_o^+ = 0.2$; Case 1): (*a*) $\alpha = 14.5°$, $t = 1.373$; (*b*) $\alpha = 19.5°$, $t = 1.809$; (*c*) $\alpha = 22.5°$, $t = 2.071$.

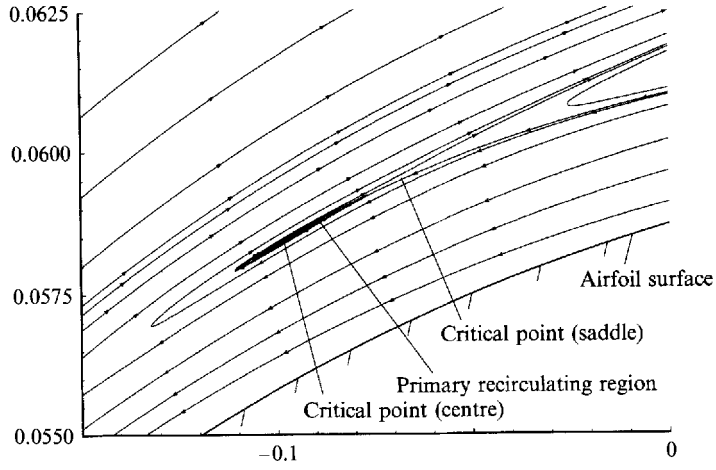

FIGURE 4. Instantaneous streamlines at $\alpha = 15°$, $t = 1.417$ ($Re_c = 10^4$, $M_\infty = 0.2$, $\Omega_o^+ = 0.2$; Case 1).

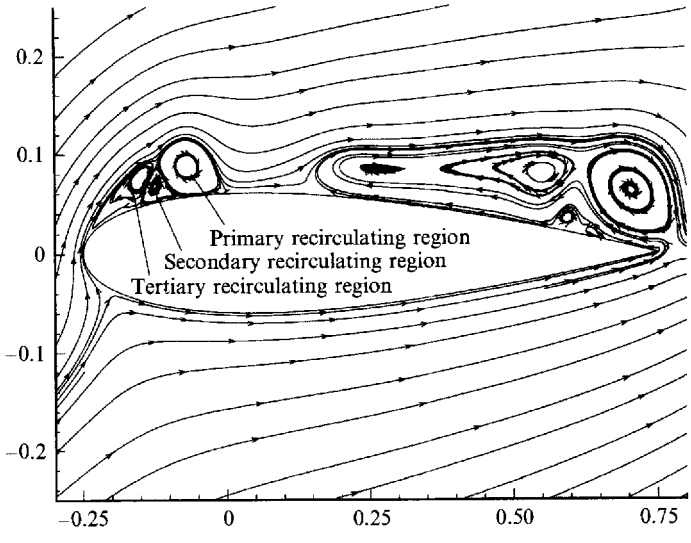

FIGURE 5. Instantaneous streamlines over the entire airfoil at $\alpha = 22.5°$, $t = 2.071$ ($Re_c = 10^4$, $M_\infty = 0.2$, $\Omega_o^+ = 0.2$; Case 1)

to the airfoil surface in a direction approximately normal to the wall, thus leading to boundary layer separation (Peridier *et al.* 1991*a*,*b*). The primary recirculating region eventually detaches from the airfoil surface and becomes the dynamic stall vortex. The developments near the leading edge are relatively isolated from the developments on the aft portion of the airfoil by a region of attached flow (figure 5).

3.2. *Case 2* : $Re_c = 10^4$, $M_\infty = 0.2$, $\Omega_o^+ = 0.1$

The instantaneous streamlines are shown in figure 6(*a*,*b*) for $\alpha = 15°$ and 17°, respectively. At $\alpha = 15°$, the primary recirculating region is seen. The clockwise-rotating primary recirculating region forms at $\alpha = 14.29°$ ($t = 2.600$) at 27% chord and a distance $1.25 \times 10^{-2}c$ above the wall. At $\alpha = 17°$, a counterclockwise-rotating secondary recirculating region forms below the primary recirculating region at the 16% chord position. The primary recirculating region has grown normal to the airfoil

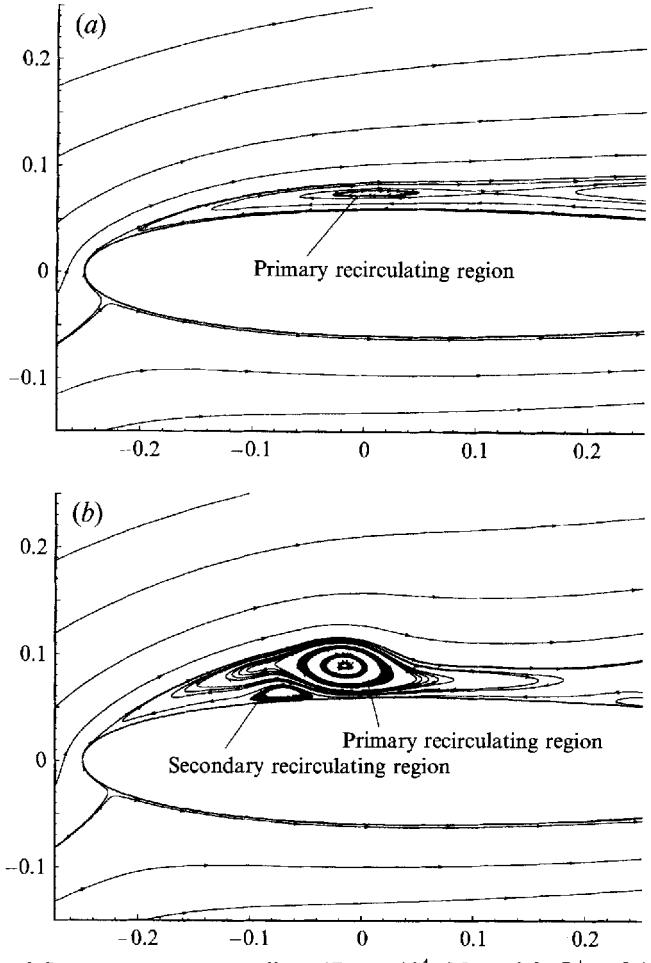

FIGURE 6. Instantaneous streamlines ($Re_c = 10^4$, $M_\infty = 0.2$, $\Omega_o^+ = 0.1$; Case 2): (*a*) $\alpha = 15°$, $t = 2.725$; (*b*) $\alpha = 17°$, $t = 3.074$.

surface and also moved toward the leading edge. The instantaneous streamlines at $\alpha = 18°$ (not shown here) indicate the development of a clockwise-rotating tertiary recirculating region on top of the secondary recirculating region in between the leading edge and the primary recirculating region. The flow structures are similar to Case 1 ($\Omega_o^+ = 0.2$). However, the primary recirculating region appears at a smaller angle as compared to Case 1. Also, the structures form farther away from the leading edge and toward the trailing edge on the upper surface in Case 2.

3.3. *Case 3* : $Re_c = 10^4$, $M_\infty = 0.2$, $\Omega_o^+ = 0.05$

The instantaneous streamlines over the entire airfoil are shown in figure 7(*a–c*) for $\alpha = 10.5°$, 12°, and 13.5°, respectively. The reversed flow extends over the entire airfoil upper surface at $\alpha = 10.5°$. The trailing-edge recirculating region stretches along the airfoil upper surface and breaks down into multiple recirculating regions at $\alpha = 12°$ extending over the entire airfoil top surface. Unlike Cases 1 and 2 (which are at a higher pitch rate), the flow developments near the trailing edge are not isolated from the developments near the leading edge. Also, the recirculating regions appear far from the wall (average distance of $4.0 \times 10^{-2}c$). The instantaneous streamlines at $\alpha = 13.5°$ demonstrate the increase in size of the multiple recirculating regions in the

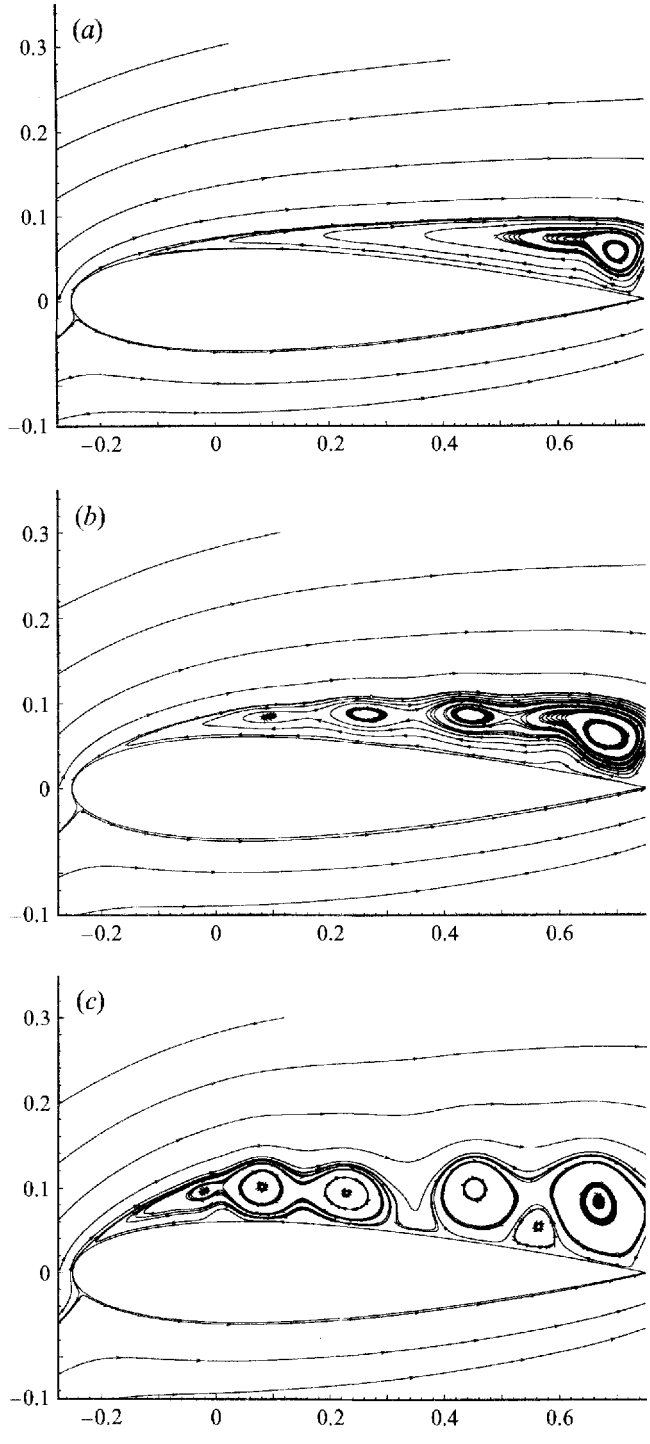

FIGURE 7. Instantaneous streamlines ($Re_c = 10^4$, $M_\infty = 0.2$, $\Omega_o^+ = 0.05$; Case 3): (*a*) $\alpha = 10.5°$, $t = 3.773$; (*b*) $\alpha = 12°$, $t = 4.296$; (*c*) $\alpha = 13.5°$, $t = 4.820$.

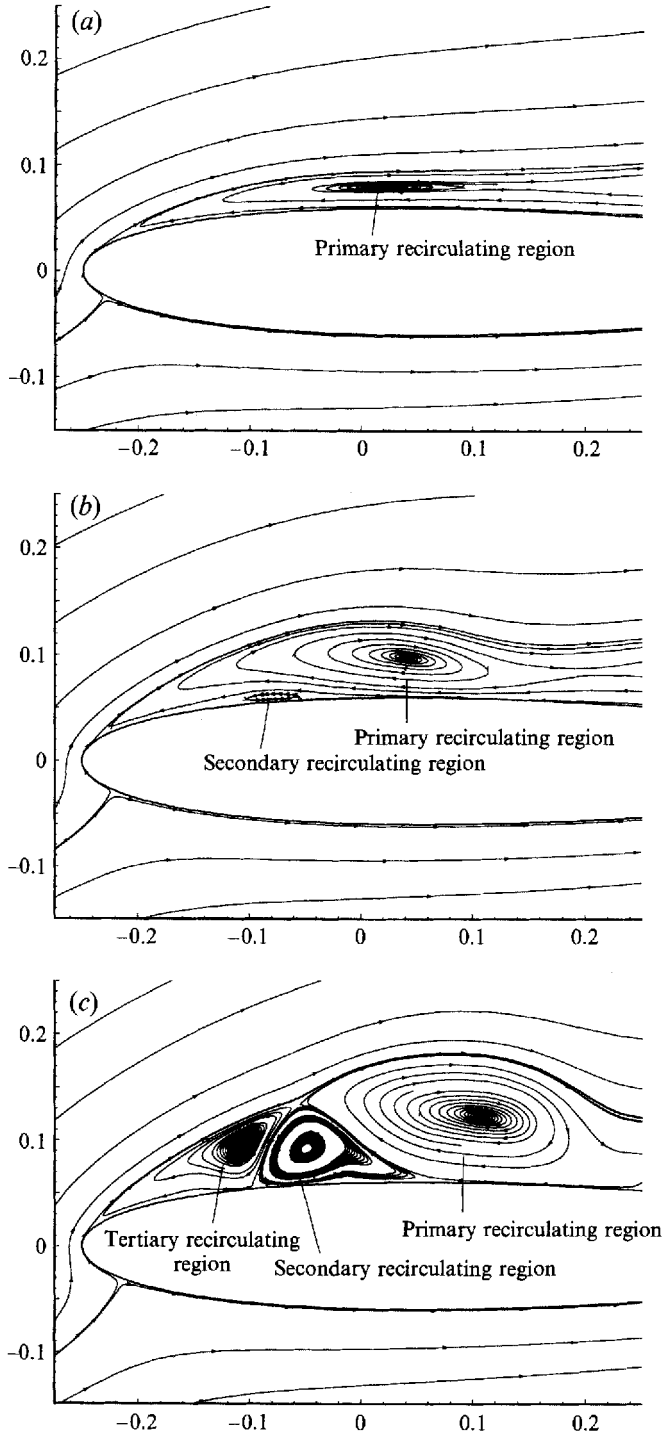

FIGURE 8. Instantaneous streamlines ($Re_c = 10^4$, $M_\infty = 0.5$, $\Omega_o^+ = 0.2$; Case 4): (*a*) $\alpha = 19.5°$, $t = 1.809$; (*b*) $\alpha = 22.5°$, $t = 2.071$; (*c*) $\alpha = 25.5°$, $t = 2.332$.

transverse direction with increase in the angle of attack, giving rise to breakdown of the entire upper-surface boundary layer. The development of the flow structure which gives rise to the dynamic stall vortex is not isolated in the leading edge only and appears over the entire airfoil upper surface, which is different from Cases 1 and 2.

3.4. *Case 4* : $Re_c = 10^4$, $M_\infty = 0.5$, $\Omega_o^+ = 0.2$

The instantaneous streamlines over the front 50% of the airfoil are shown in figure 8(*a–c*) for $\alpha = 19.5°$, 22.5°, and 25.5°, respectively. The reversed flow region observed over the airfoil upper surface for this case is much thicker than the reversed flow region at $M_\infty = 0.2$ (Cases 1 and 2). At $\alpha = 19.5°$, the primary recirculating region has formed; it appears first at $\alpha = 18.8°$ ($t = 1.748$) at the 30% chord position and a distance $1.7 \times 10^{-2}c$ from the airfoil surface. The secondary recirculating region can be seen at $\alpha = 22.5°$; it develops below the primary recirculating region which expands normal to airfoil surface. At $\alpha = 25.5°$, the tertiary recirculating region appears above the secondary recirculating region and the primary recirculating region is pushed farther from the airfoil surface. In this case, the vortical structures have a larger length scale than Case 1 or Case 2. Again, the development of the flow field is very similar to Cases 1 and 2, but with a delay.

3.5. *Case 5* : $Re_c = 10^4$, $M_\infty = 0.5$, $\Omega_o^+ = 0.1$

The instantaneous streamlines at $\alpha = 15°$, 16.5°, 18°, and 19.5° over the leading 70% of the airfoil are shown in figure 9(*a–d*). At $\alpha = 15°$, a thick reversed flow region is observed over the entire upper surface. The primary recirculating originates at $\alpha = 15.65°$ ($t = 2.839$) at the 44% chord position and a distance $3.8 \times 10^{-2}c$ above the airfoil surface. The primary recirculating region is observed to have developed at $\alpha = 16.5°$, and the secondary recirculating region forms below the primary recirculating region ($\alpha = 18°$). At $\alpha = 19.5°$, the tertiary recirculating region can be seen. The secondary recirculating region separates the primary recirculating region from the tertiary recirculating region. The separation process is again observed to be similar to Cases 1, 2, and 4. The principal differences are that the structures form farther away from the leading edge compared to the other three cases, and the length scale associated with the flow structures is substantially greater.

3.6. *Case 6* : $Re_c = 10^4$, $M_\infty = 0.5$, $\Omega_o^+ = 0.05$

The instantaneous streamlines over the entire airfoil upper surface are shown in figure 10(*a–c*) for $\alpha = 12°$, 13.5°, and 15°, respectively. At $\alpha = 12°$, two separate recirculating regions are present near the trailing edge and the reversed flow extends over the entire airfoil upper surface. The fore recirculating region forms from the breakup of the trailing-edge recirculating region. The recirculating region attached at the trailing edge is shed in the wake at $\alpha = 13.5°$, while the other one expands and is still attached to the airfoil surface. With increase in α to 15° two more recirculating regions appear. The development of the flow structures in this case resembles Cases 1, 2, 4, and 5. However, the flow structures are not confined to only a part of the airfoil upper surface: the primary recirculating region appears near the trailing edge and extends over the entire airfoil surface before breaking down into secondary and tertiary recirculating regions.

3.7. *Case 7* : $Re_c = 10^5$, $M_\infty = 0.5$, $\Omega_o^+ = 0.2$

The instantaneous streamlines are presented for $\alpha = 15°$, 18°, 19°, and 19.5° in figure 11(*a–d*). The instantaneous streamlines at $\alpha = 15°$ (figure 11) show the presence

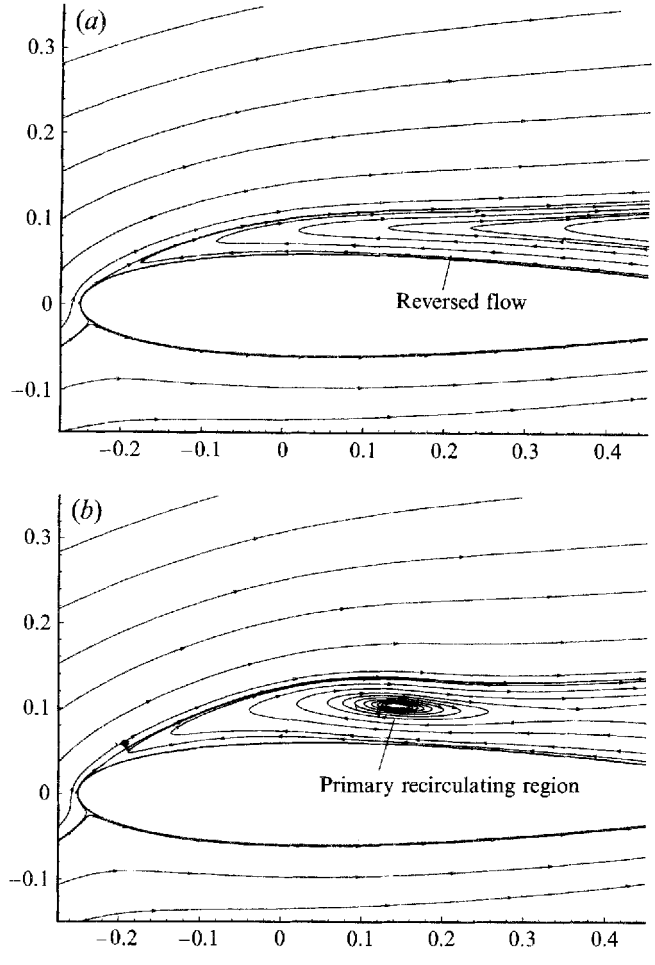

FIGURE 9 (*a*, *b*). For caption see facing page.

of the primary recirculating region near the leading edge in the close-up figure of the boxed region; it forms at $\alpha = 14.9°$ ($t = 1.407$) as compared to $\alpha = 18.8°$ for Case 4, and expands in a direction normal to airfoil surface with increase in α. This can be observed at $\alpha = 18°$. At $\alpha = 19°$, the secondary and tertiary recirculating regions are also evident. Up to $\alpha = 19°$, the development of the flow field is very similar to Cases 1, 2, 4, 5 and 6. However, at $\alpha = 19.5°$, multiple recirculating regions are seen attached to the airfoil surface. Similar results have been reported in an analytical study by Smith (1982) and in a numerical study by Ghia *et al.* (1992) at $Re_c = 4.5 \times 10^4$, where the simultaneous appearance of multiple recirculating regions near the leading edge at high Reynolds numbers was found. The pressure coefficient contours at $\alpha = 18°$, and 19.5° in figure 12(*a*,*b*), respectively, show the appearance of a shock in the flow field at $\alpha = 19.5°$. Examination of the Mach contours and the divergence of velocity in the flow field (not shown here) also indicate a shock, which appears between $\alpha = 19°$ and $\alpha = 19.5°$. A separate inviscid computation similarly showed the appearance of a shock near the leading edge, which proves that the shock appearance is an inviscid phenomenon. For the inviscid case, the shock appears at a smaller angle of attack and nearer to the leading edge than in the viscous case. The length scale associated

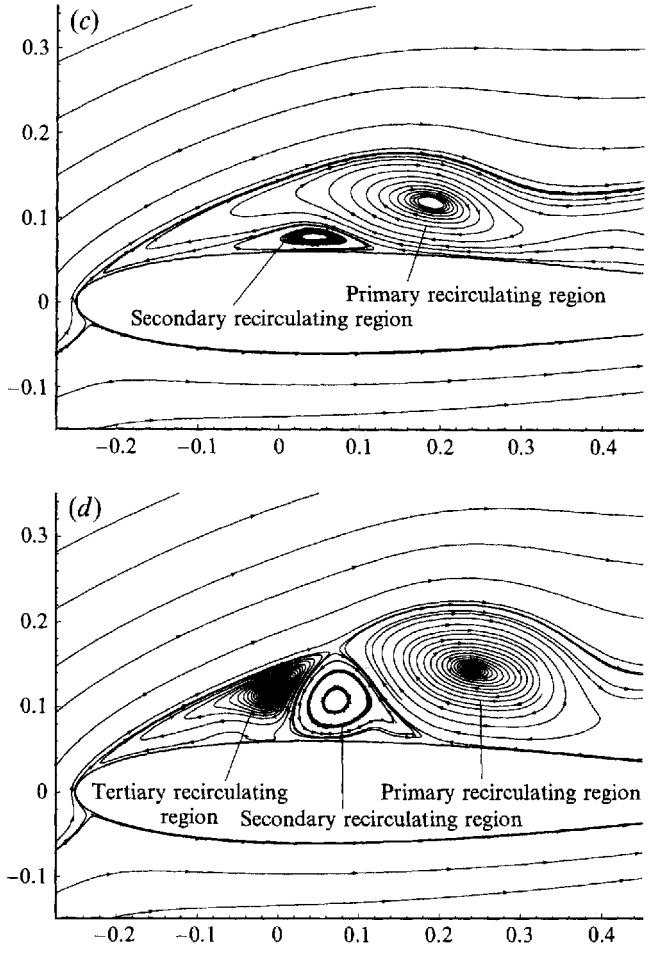

FIGURE 9. Instantaneous streamlines ($Re_c = 10^4$, $M_\infty = 0.5$, $\Omega_0^+ = 0.1$; Case 5): (*a*) $\alpha = 15°$, $t = 2.725$; (*b*) $\alpha = 16.5°$, $t = 2.987$; (*c*) $\alpha = 18°$, $t = 3.249$; (*d*) $\alpha = 19.5°$, $t = 3.511$.

with the recirculating regions in this case is observed to be very small as compared to those in the other cases.

3.8. *Effect of compressibility*

The results indicate important trends related to the increase in Mach number. In Cases 1 and 4, 2 and 5, the pitch rate and Reynolds number are fixed while the Mach number is increased from 0.2 to 0.5. Increasing the Mach number (at fixed Reynolds number and pitch rate) causes the primary recirculating region to form farther from the airfoil surface and delays its formation. Sankar & Tassa (1981) also saw a delay in the formation of the 'leading edge vortex' (primary recirculating region) when the Mach number was increased from 0.2 to 0.4 at $Re_c = 5.0 \times 10^3$. Figure 13 displays the angle at which the primary recirculating region first appears as a function of the pitch rate for two different Mach numbers at $Re_c = 10^4$. At a constant pitch rate, the formation of the primary recirculating region is delayed to higher angles when the Mach number is increased from 0.2 to 0.5. The surface pressure coefficient was compared to study the effect of Mach number. Figure 14 shows that for a fixed pitch rate and Reynolds number, increasing the Mach number causes a decrease in

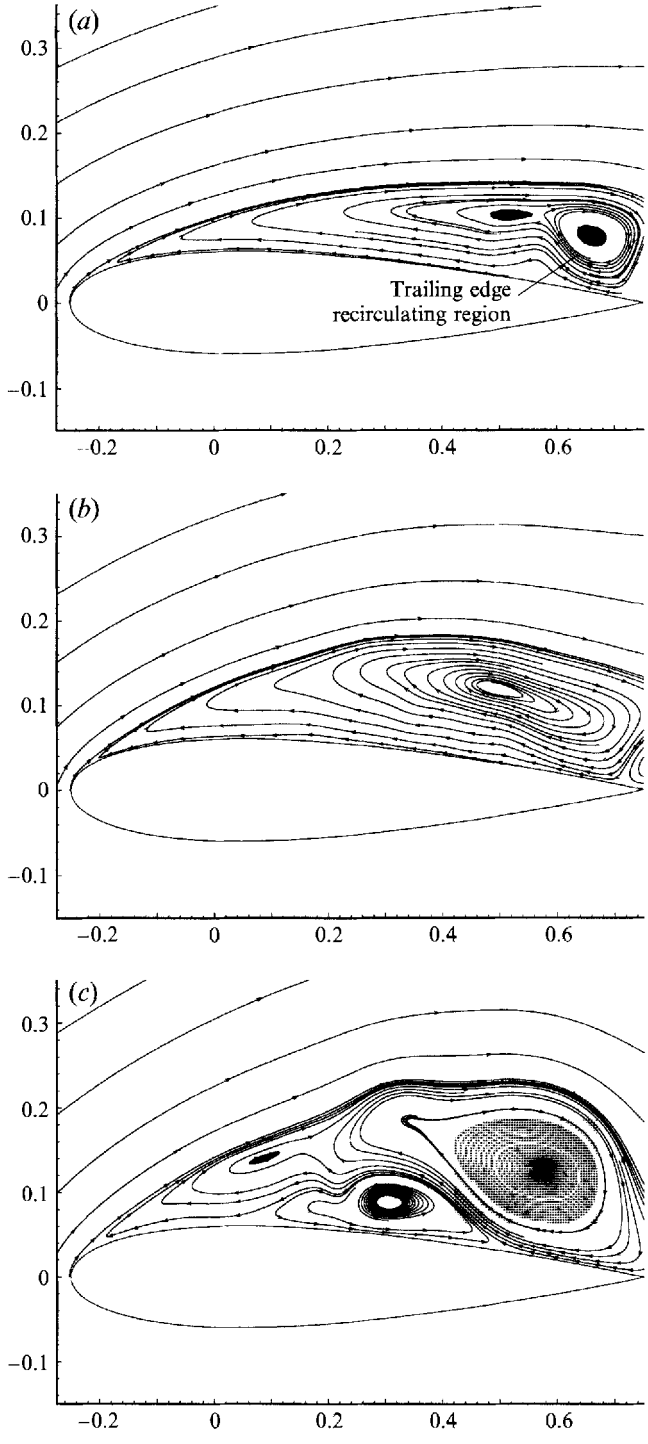

FIGURE 10. Instantaneous streamlines ($Re_c = 10^4$, $M_\infty = 0.5$, $\Omega_o^+ = 0.05$; Case 6): (*a*) $\alpha = 12°$, $t = 4.296$; (*b*) $\alpha = 13.5°$, $t = 4.820$; (*c*) $\alpha = 15°$, $t = 5.343$.

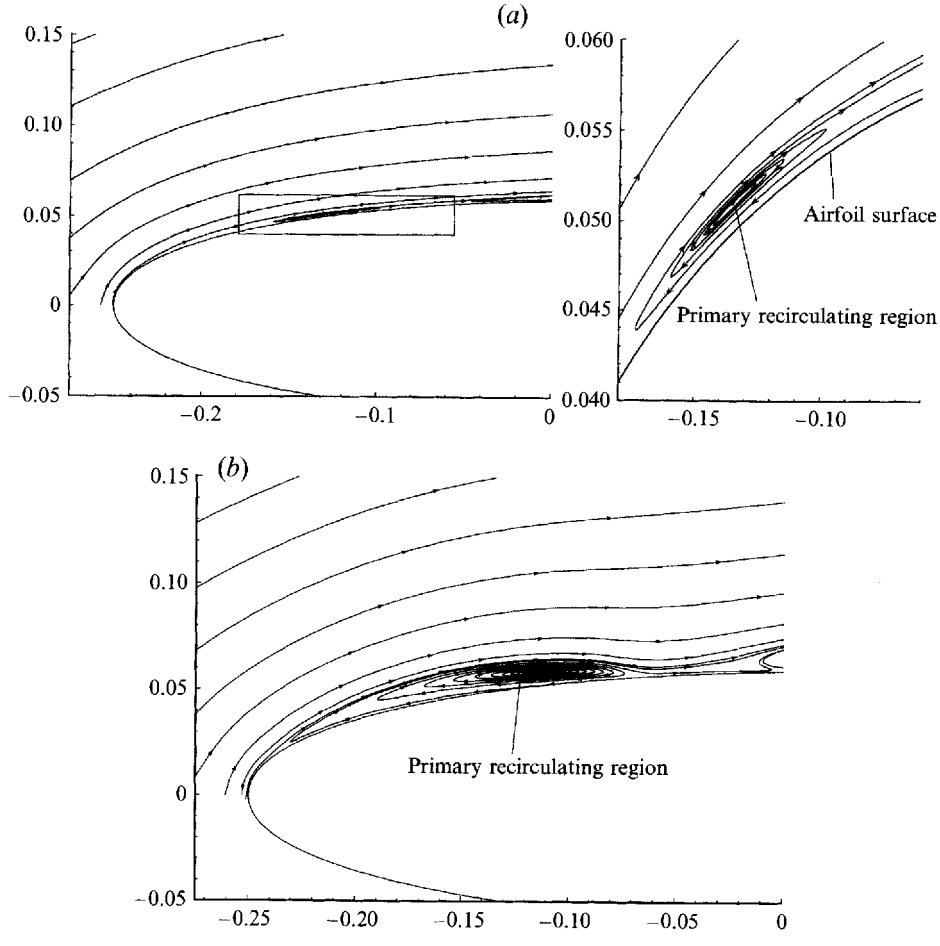

FIGURE 11 (*a, b*). For caption see next page.

the leading-edge suction pressure coefficient which in turn results in a lower adverse pressure gradient on the airfoil upper surface. The decreased adverse pressure gradient on the top surface at higher Mach numbers retards the movement of the reversed flow region toward the leading edge but increases the thickness of the reversed flow region and eventually delays the formation of the primary recirculating region. The length scale associated with the flow structures increase as well. The decrease in the magnitude of the leading-edge suction pressure coefficient is primarily due to the compressibility effects on the boundary layer, which increase the effective radius of the leading edge of the airfoil. This is opposite to the behaviour expected from a quasi-stationary application of the Prandtl–Glauert rule, where $C_{p_M}/C_{p_i} = 1/(1 - M^2)^{1/2}$ (C_{p_M} is the pressure coefficient for a compressible case of Mach number M and C_{p_i} is the pressure coefficient for an incompressible case).

3.9. *Effect of pitch rate*

The flow field is strongly dependent on the pitch rate. Comparison of Cases 1, 2 and 3, or 4, 5 and 6 exhibits the effects of the pitch rate at a fixed Mach number and Reynolds number. The pitch rate is decreased from 0.2 to 0.05 in cases 1–3 and 4–6. Increasing in the pitch rate of the airfoil delays the formation of the primary

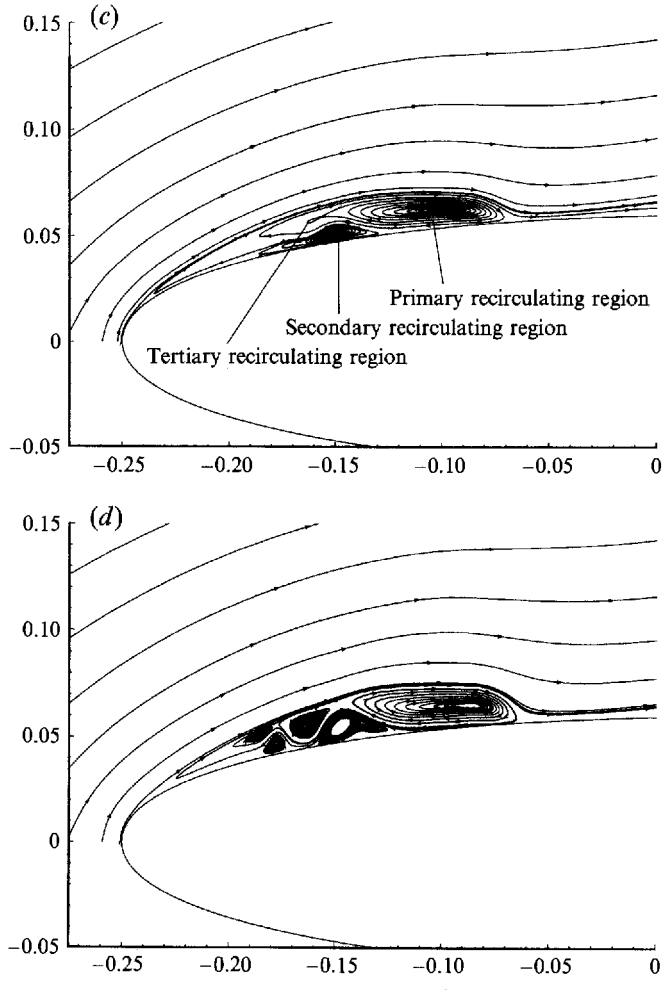

FIGURE 11. Instantaneous streamlines ($Re_c = 10^5$, $M_\infty = 0.5$, $\Omega_o^+ = 0.2$; Case 7): (*a*) $\alpha = 15°$, $t = 1.417$; (*b*) $\alpha = 18°$, $t = 1.678$; (*c*) $\alpha = 19°$, $t = 1.765$; (*d*) $\alpha = 19.5°$, $t = 1.809$.

recirculating region to higher angles of attack. The primary recirculating region forms closer to the leading edge on the upper surface. It is also observed that a decrease in the pitch rate causes the transition from a predominantly leading-edge separation to a complex separation over the entire airfoil. Figure 13 shows the delay in the formation of the recirculating region with increase in pitch rate at constant Mach number and $Re_c = 10^4$. It should be noted that the delay in the formation of the recirculating region to higher angles does not mean that there is an increase in the actual time from start of pitch-up to the appearance of the recirculating region (the pitch rate is different). At higher pitch rates, there is a decrease in the adverse pressure gradient on the upper surface of the airfoil (figure 15), which slows down the development of the reversed flow region and delays the appearance of the primary recirculating region to a higher angle.

3.10. *Effect of Reynolds number*

The flow field is sensitive to the change in Reynolds number. Cases 4 and 7 are compared to study the effect of an increase in Reynolds number at a fixed Mach

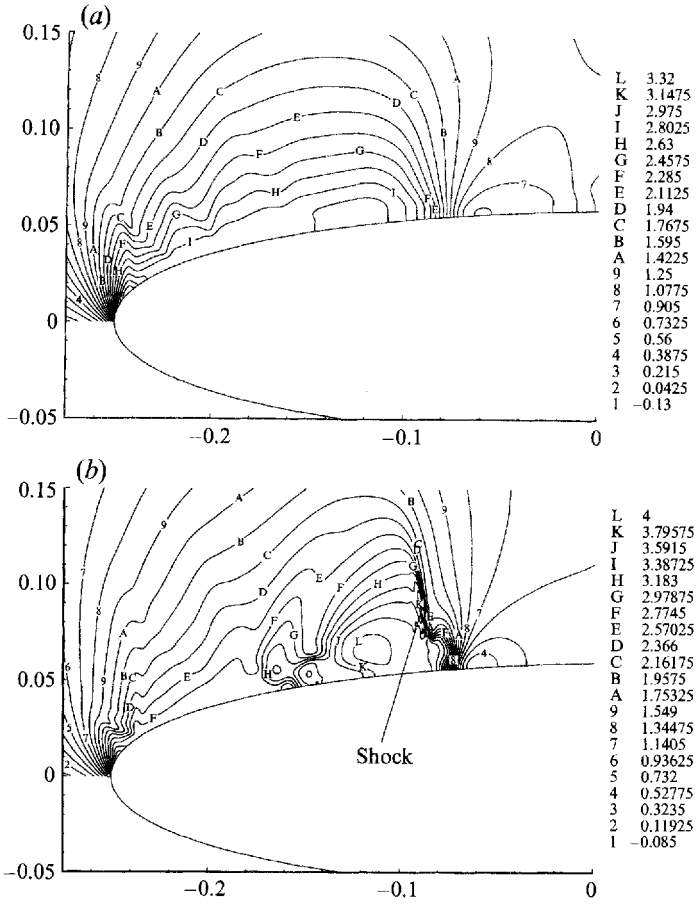

FIGURE 12. Pressure coefficient contours ($Re_c = 10^5$, $M_\infty = 0.5$, $\Omega_o^+ = 0.2$; Case 7): (*a*) $\alpha = 18°$; (*b*) $\alpha = 19.5°$.

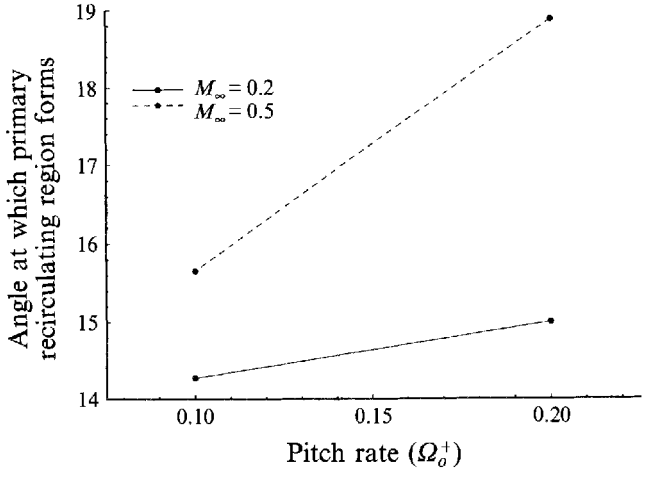

FIGURE 13. Effect of Mach number and pitch rate on the appearance of the primary recirculating region at $Re_c = 10^4$.

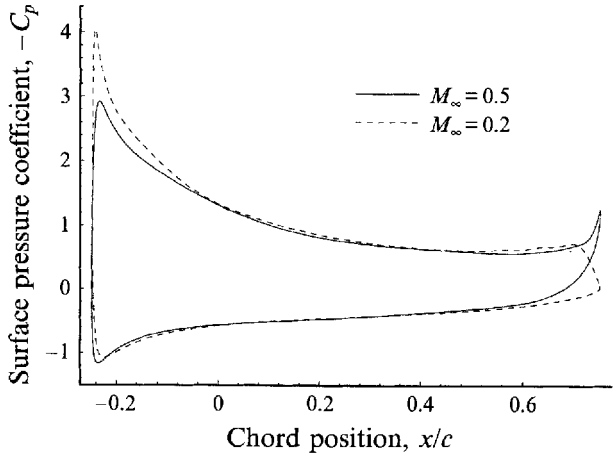

FIGURE 14. Comparison of the surface pressure coefficient at $\alpha = 16.5°$ for two different Mach numbers ($Re_c = 10^4$, $\Omega_o^+ = 0.2$).

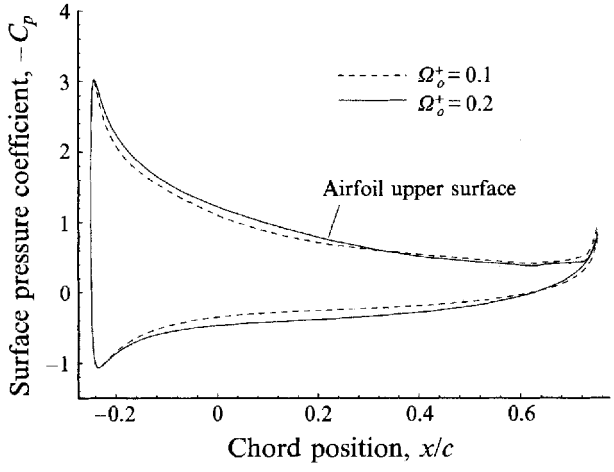

FIGURE 15. Comparison of the surface pressure coefficient at $\alpha = 13.5°$ for two different pitch rates ($Re_c = 10^4$, $M_\infty = 0.2$).

number and pitch rate. Increasing the Reynolds number hastens the appearance of the primary recirculating region and decreases the length scale of the flow structures. The primary recirculating region forms closer to the leading edge on the upper surface at higher Reynolds number. At $Re_c = 10^5$ amd $M_\infty = 0.5$, a shock appears on the top surface. The appearance of the shock was found to be an inviscid phenomenon. Multiple recirculating regions develop simultaneously near the leading edge at higher Reynolds number and cause a complex separation of the boundary layer. Up to the formation of the shock, the evolution of the flow field is identical in both cases except for the lag. The formation of the recirculating regions near the leading edge is not induced by the shock. Chandrasekhara *et al.* (1994) observed the presence of similar shocks near the leading edge at $M_\infty = 0.45$ and $Re_c = 3.6 \times 10^5$, in experiments.

Case	Memory (Mw)	CPUtime (in hours)	
		'Steady' state at $\alpha = 0°$	Pitching motion
1c	9.8	5†	2
2b	34	34	12
3b	34	‡	19
4b	34	21	7
5b	34	‡	12
6b	60	51	36
7b	128	103	22

† The flowfield at $\alpha = 0°$ is not precisely steady, since there is periodic vortex shedding from the trailing edge. The figures listed represent the CPU time required to achieve the periodic state.
‡ Separate computation of 'steady' state not required.

TABLE 3. CPU and memory requirements for the computations on a Cray C90

3.11. *Code performance*

The Navier–Stokes solver is fully vectorized and was run on the Cray C90. Some typical CPU time and memory requirements for the computations are shown in table 3. The solver has a sustained performance of approximately 380 MFLOPS.

4. Conclusions

The effects of compressibility, pitch rate and Reynolds number on the initial stages of boundary layer separation on a NACA-0012 airfoil pitching about its quarter-chord position have been studied numerically. The principal results of the study are as follows.

(i) Mach number

Increasing the Mach number from 0.2 to 0.5 (at fixed Reynolds number and pitch rate) delays the formation of the primary recirculating region and causes it to form farther from the airfoil surface. The compressibility effects on the boundary layer result in a decrease in the magnitude of the leading-edge suction pressure coefficient and a consequent decrease in the adverse pressure gradient on the upper surface. The decrease in adverse pressure gradient retards the movement of the reversed flow region towards the leading edge and hence delays the formation of the primary recirculating region.

(ii) Pitch rate

Increasing the pitch rate from 0.05 to 0.2 (at fixed Mach number and Reynolds number) causes the transition from trailing-edge separation to leading-edge separation.

Increasing the pitch rate delays the formation of the primary recirculating region to higher angles of attack. This is due to the decrease in the adverse pressure gradient on the airfoil upper surface which retards the development of the reversed flow region on the upper surface and the formation of the primary recirculating region. The primary recirculating region also appears closer to the leading edge.

(iii) Reynolds number

Increasing the Reynolds number from 10^4 to 10^5 (at fixed Mach number and pitch rate) hastens the appearance of the primary recirculating region and decreases the length scale of the flow structures.

Multiple recirculating regions appear simultaneously near the leading edge.

(iv) Shock wave

A shock appears on the top surface at $Re_c = 10^5$, $M_\infty = 0.5$, and $\Omega_o^+ = 0.2$ at $\alpha = 19.5°$. A separate inviscid computation also showed a similar appearance of shock, implying that the formation of the shock is an inviscid phenomenon. For the inviscid case, the shock appears closer to the leading edge and also at a smaller angle of attack compared to the viscous case.

The formation of the recirculating regions near the leading edge was found not to be induced by the shock.

This research was sponsored by the Army Research Office under Grant DAAL03-91-G-0096, monitored by Dr Tom Doligalski. The authors gratefully acknowledge the valuable suggestions from Drs Larry Carr, M. S. Chandrasekhara, Tom Doligalski, Miguel Visbal, Abdelfattah Zebib, and Mr Cedric Lecunff. Supercomputing resources have been provided by the NASA Ames Research Center and the DOD High Performance Computing Center (USAE Waterways Experiment Station). The results have been analysed at the Rutgers University Supercomputer Remote Access Center.

REFERENCES

ACHARYA, M. & METWALLY, M. 1990 Evolution of the unsteady pressure field and vorticity production at the surface of a pitching airfoil. *AIAA Paper* 90-1472.

BEAM, R. M. & WARMING, R. F. 1978 An implicit factored scheme for the compressible Navier-Stokes equations. *AIAA J.* **16**, 393–402.

CARR, L. 1988 Progress in analysis and prediction of dynamic stall. *J. Aircraft* **25**, 6–17.

CARR, L. & CHANDRASEKHARA, M. S. 1995 An assessment of the impact of compressibility on dynamic stall. *AIAA Paper* 95–0779.

CARR, L. & MCCROSKEY, W. 1992 A review of recent advances in computational and experimental analysis of dynamic stall. *IUTAM Symp. on Fluid Dynamics of High Angle of Attack.*

CHANDRASEKHARA, M. S. & AHMED, S. 1991 Laser velocimetry measurements of oscillating airfoil dynamic stall flow field. *AIAA Paper* 91–1799.

CHANDRASEKHARA, M. S., CARR, L. W. & WILDER, M. C. 1994 Interferometric investigations of compressible dynamic stall over a transiently pitching airfoil. *AIAA J.* **32**, 586–593.

CRISLER, W., KROTHAPALLI, A. & LOURENCO, L. 1994 PIV investigation of high speed flow over a pitching airfoil. *AIAA Paper* 94–0533.

CURRIER, J. M. & FUNG, K. Y. 1992 Analysis of the onset of dynamic stall. *AIAA J.* **30**, 2469–2477.

DOLIGALSKI, T. L., SMITH, C. R. & WALKER, J. D. A. 1994 Vortex interactions with walls. *Ann. Rev. Fluid Mech.* **26**, 573–616.

GHIA, K. N., YANG, J., OSSWALD, G. A. & GHIA, U. 1992 Study of the role of unsteady separation in the formation of dynamic stall vortex. *AIAA Paper* 92–0196.

GHOSH CHOUDHURI, P., KNIGHT, D. & VISBAL, M. 1994 Two-dimensional unsteady leading-edge separation on a pitching airfoil. *AIAA J.* **32**, 673–681.

KARIM, MD. A. 1992 Experimental investigation of the formation and control of the dynamic-stall vortex over a pitching airfoil. MS thesis, Illinois Institute of Technology.

KINSEY, D. & BARTH, T. 1984 Description of a hyperbolic grid generating procedure for arbitrary two dimensional bodies. *AFWAL-TM*-84-191.

MCCROSKEY, W., CARR, L. & MCALISTER, K. 1976 Dynamic stall experiments on oscillating airfoils. *AIAA J.* **14**, 57–63.

MEHTA, U. 1977 Dynamic stall of an oscillating airfoil. *AGARD CP*–227.

PERIDIER, V, SMITH, F. & WALKER, J. 1991*a* Vortex-induced boundary layer separation. Part 1. The limit problem $Re \rightarrow \infty$. *J. Fluid Mech.* **232**, 99–131.

PERIDIER, V., SMITH, F. & WALKER, J. 1991*b* Vortex-induced boundary layer separation. Part 2. Unsteady interacting boundary layer theory. *J. Fluid Mech.* **232**, 133–165.

PULLIAM T. H. 1986 Artificial dissipation models for the euler equations. *AIAA J.* **24**, 1931–1940.

SANKAR, N. L. & TASSA, Y. 1981 Compressibility effects on dynamic stall of an NACA-0012 airfoil. *AIAA J.* **19**, 557–558.

SHIH, C., LOURENCO, L., VAN DOMMELEN, L. & KROTHAPALLI, A. 1992 Unsteady flow past an airfoil pitching at a constant rate. *AIAA J.* **30**, 1153–1161.

SMITH, F. T. 1982 Concerning dynamic stall. *Aero. Q.* **33**, 331–352.

SMITH, F. T. 1988 Finite-time break-up can occur in any unsteady interacting boundary layer. *Mathematika* **35**, 256–273.

SMITH, F. T. & ELLIOTT, J. W. 1985 On the abrupt turbulent reattachment downstream of leading-edge laminar separation. *Proc. R. Soc. Lond.* A **401**, 1–27.

STEGER, J. 1978 Implicit finite-difference simulation of flow about arbitrary two-dimensional geometries. *AIAA J.* **16**, 679–686.

STEGER, J. & CHAUSSEE, D. 1980 Generation of body-fitted coordinates using hyperbolic partial differential equations. *SIAM J. Sci. Statist. Comput.* **1**, 431–437.

THOMAS, J. & SALAS, M. 1986 Far field boundary conditions for transonic lifting solutions to the Euler equations. *AIAA J.* **24**, 1074–1080.

THOMAS, P. & LOMBARD, C. 1979 Geometric conservation law and its applications to flow computations on moving grids. *AIAA J.* **17**, 1030–1037.

VAN DOMMELEN, L. L. & SHEN, S. F. 1980 The spontaneous generation of the singularity in a separating laminar boundary layer. *J. Comput. Phys.* **38**, 125–140.

VISBAL, M. R. 1986*a* Calculation of viscous transonic flows about a supercritical airfoil. *AFWAL TR*-86-3013.

VISBAL, M. R. 1986*b* Evaluation of an implicit Navier-Stokes solver for some unsteady separated flows. *AIAA Paper* 86–1053.

VISBAL, M. R. 1990 Dynamic stall of a constant rate pitching airfoil. *J. Aircraft* **27**, 400–407.

VISBAL, M. R. 1991 On the formation and control of the dynamic stall vortex on a pitching airfoil. *AIAA Paper* 91–0006.

VISBAL, M. R. & SHANG, J. 1989 Investigation of the flow structure around a rapidly pitching airfoil. *AIAA J.* **24**, 1044–1051.

WHITE, F. 1974 *Viscous Fluid Flow*. McGraw-Hill.

YANG, J., GHIA, K. N., GHIA, U. & OSSWALD, G. A. 1993 Management of dynamic stall phenomenon through active control of unsteady separation. *AIAA Paper* 93–3284.